

Remote Vibration Estimation Using Displaced-Phase-Center Antenna SAR for Strong Clutter Environments

Justin B. Campbell, Francisco Pérez^{ID}, Qi Wang, *Student Member, IEEE*,
Balasubramaniam Santhanam, *Senior Member, IEEE*, Ralf Dunkel,
Armin W. Doerry, Thomas Atwood, and Majeed M. Hayat, *Fellow, IEEE*

Abstract—It has been previously demonstrated that it is possible to perform remote vibrometry using synthetic aperture radar (SAR) in conjunction with the discrete fractional Fourier transform (DFrFT). Specifically, the DFrFT estimates the chirp parameters (related to the instantaneous acceleration of a vibrating object) of a slow-time signal associated with the SAR image. However, ground clutter surrounding a vibrating object introduces uncertainties in the estimate of the chirp parameter retrieved via the DFrFT method. To overcome this shortcoming, various techniques based on subspace decomposition of the SAR slow-time signal have been developed. Nonetheless, the effectiveness of these techniques is limited to values of signal-to-clutter ratio ≥ 5 dB. In this paper, a new vibrometry technique based on displaced-phase-center antenna (DPCA) SAR is proposed. The main characteristic of a DPCA-SAR is that the clutter signal can be canceled, ideally, while retaining information on the instantaneous position and velocity of a target. In this paper, a novel method based on the extended Kalman filter (EKF) is introduced for performing vibrometry using the slow-time signal of a DPCA-SAR. The DPCA-SAR signal model for a vibrating target, the mathematical characterization of the EKF technique, and vibration estimation results for various types of vibration dynamics are presented.

Index Terms—Clutter cancellation, discrete fractional Fourier transform (DFrFT), displaced-phase-center antenna (DPCA), extended Kalman filter (EKF), ground moving target indicator, micro-Doppler, synthetic aperture radar (SAR), vibrometry.

I. INTRODUCTION

SYNTHETIC aperture radar (SAR) is a ubiquitous coherent imaging radar that generates high-resolution images. SAR operates by illuminating the target scene with electromagnetic pulses, typically in the microwave band, and measures the

amplitude and phase of the return signal. After substantial signal processing of the collected data, the final product is a 2-D image, where each pixel in the image represents the reflectivity of a region at the transmitted frequency [1]. The relatively long wavelengths, compared with those of optical sensors, make SAR systems capable of remote imaging over thousands of kilometers regardless of weather conditions. The typical range of these systems can be anywhere from 25 km for the Lynx radar [2] to well over 800 km for the RADARSAT-2 [3]. These SAR-collection platforms can generate images at a variety of resolution scales. For example, the Lynx radar has the ability to generate 0.1-m (4-in) resolution images [2].

For common imaging applications, a typical airborne SAR platform illuminates the ground scene for at least several seconds to create a single SAR image. During the data-collection process, the image formation algorithm, often the polar-format algorithm, assumes all targets in the ground scene are static. This assumption makes SAR particularly sensitive to low-level target vibrations [4]–[11]. More specifically, ground target vibrations introduce a phase modulation, termed the micro-Doppler effect [8], into each returned SAR signal. Any vibrating target, with a strong radar cross section relative to its surroundings, will produce observable artifacts in the image called ghost targets. These ghost targets degrade the image quality. An example of these ghost targets is shown in Fig. 1. On the other hand, while ground target vibrations may introduce distortion in some regions of a SAR image [4], [8], they contain vital information about the frequency and amplitude of the vibration of a target. In turn, the vibration history, if reliably detected, can aid the identification of the targets imaged.

Previously, a vibration-estimation technique was introduced based on the discrete fractional Fourier transform (DFrFT) applied to the slow-time SAR signal, which is extracted from the complex SAR image [12]–[15]. It has been shown that the DFrFT method can accurately estimate the instantaneous acceleration of a point target when the vibration of interest occurs in the range direction [12]–[15]. In these cases, the micro-Doppler effect manifests itself as an instantaneous linear chirp in the SAR slow-time signal [12]–[15].

While the DFrFT is an effective remote vibration-estimation tool, the reliability of its estimates is adversely affected by the

Manuscript received February 22, 2017; revised September 11, 2017; accepted December 1, 2017. Date of publication January 1, 2018; date of current version April 20, 2018. This work was supported by the U.S. Department of Energy under Award DE-NA0002494. (*Corresponding author: Francisco Pérez.*)

J. B. Campbell, F. Pérez, Q. Wang, B. Santhanam, and M. M. Hayat are with the Center for High Technology Materials, Electrical and Computer Engineering Department, The University of New Mexico, Albuquerque, NM 87106 USA (e-mail: franperez@unm.edu).

R. Dunkel is with General Atomics Aeronautical Systems, Inc., Poway, CA 92121 USA.

A. W. Doerry and T. Atwood are with the Center for High Technology Materials, Electrical and Computer Engineering Department, The University of New Mexico, Albuquerque, NM 87106 USA, and also with the Sandia National Laboratories, Albuquerque, NM 87123 USA.

Color versions of one or more of the figures in this paper are available online at <http://ieeexplore.ieee.org>.

Digital Object Identifier 10.1109/TGRS.2017.2782621

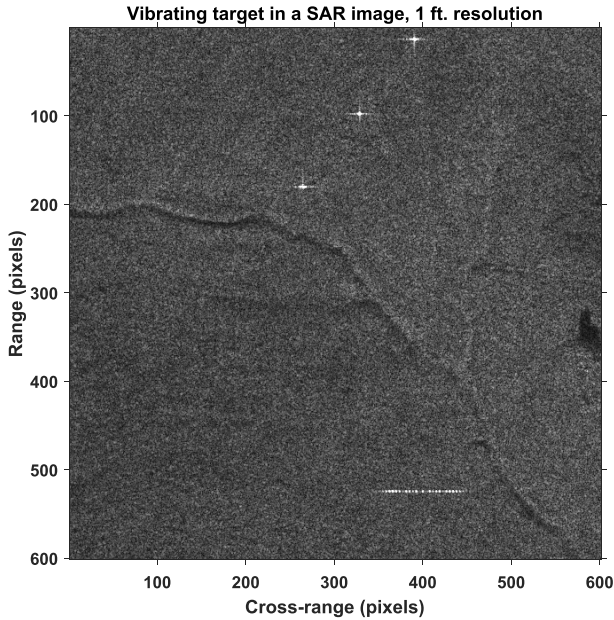


Fig. 1. SAR image that was generated by the GA-ASI Lynx SAR in collaboration with the University of New Mexico for various vibrometry experiments. Located in the bottom-right part of the image is a vibrating corner reflector with a lateral length of 0.53 m. This target had a vibration amplitude in the range direction of 1.5 cm and a vibration frequency of 0.8 Hz. The ghost targets are spread in azimuth at the same range line. The other three bright spots in the image are static corner reflectors.

ground clutter surrounding the vibrating target, e.g., requiring SAR images with signal-to-clutter ratio (SCR) ≥ 15 dB [16]. In order to overcome this shortcoming, clutter rejection techniques, based on decomposition of the SAR slow-time signal into subspaces, have been developed [16], [17]. By employing these techniques, the DFrFT can produce reliable estimates of the vibrations of targets in environments with SCR ≥ 5 dB [17]. To the best of our knowledge, there is no vibration-estimation technique based on SAR imaging that works reliably for high-clutter environments, i.e., ≤ 5 dB. Fortunately, there is an alternative radar-sensing technique, based on displaced-phase-center antenna (DPCA) systems, that is intrinsically insensitive to ground-field clutter.

The DPCA systems, normally utilized for ground moving target indication (DPCA-GMTI), have been shown to be capable of determining the position and velocity of a moving target in a high clutter environment [3]. In fact, in a DPCA-GMTI system, the return of all the static objects in the scene can be canceled by properly processing the return signals acquired by the fore-antenna and the aft-antenna. Typically, the data collection process of a DPCA-GMTI system lasts fractions of seconds, but in a SAR, it may last several seconds or more. Therefore, in order to have the Doppler resolution of a SAR image with the clutter suppression capability offered by the DPCA-GMTI system, this paper proposes performing DPCA-GMTI using SAR. The acronym DPCA-SAR is used to represent this process. A DPCA-SAR can be seen as a single-pass collection platform where, in effect, two SAR images, having only a temporal separation, are combined to provide a ground moving target indicator system. A notable

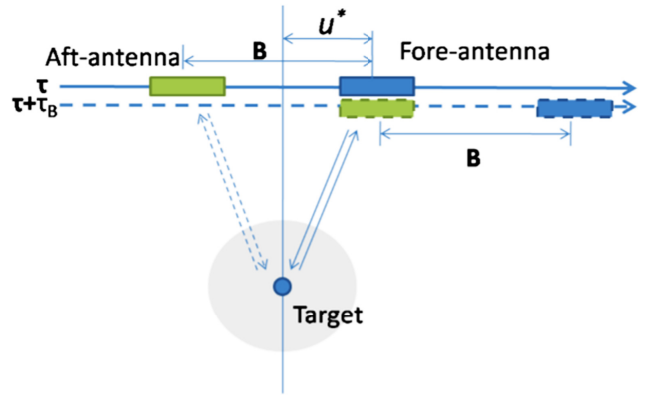


Fig. 2. Data-collection geometry of the DPCA-SAR operating in ping-pong mode. The baseline, B , is defined as the distance between the fore-antenna and the aft-antenna. The aft-antenna collects the data from the same points as the fore-antenna with a time delay of $\tau_B = B/V_a$.

advantage over spotlight-mode SAR is that DPCA-SAR systems are robust for detecting moving targets in high clutter environments, since the ground clutter can be completely removed from the SAR images captured by the two antennas. Thus, DPCA-SAR is a particularly appealing platform for SAR vibrometry. In fact, DPCA and other multichannel techniques for detecting vibrating targets have been previously reported and their ability to suppress stationary clutter is well established [18]–[21]. Herein we proceed with DPCA-SAR for clutter suppression, choosing it for its simplicity and effectiveness. However, while DPCA-SAR is robust in high clutter environments, the process of combining the two images to remove the static background (clutter) also removes the instantaneous linear chirp of the SAR slow-time signal. Without this linear chirp characteristic, the DFrFT cannot be utilized for performing vibrometry. Therefore, an alternative vibrometry technique is required for a DPCA-SAR platform. In this paper, a vibrometry technique based on the extended Kalman filter (EKF) is developed for DPCA-SAR.

The rest of this paper is organized as follows. In Section II, the signal model for the DPCA-SAR system is defined. In Section III, an existing vibrometry technique for DPCA-SAR is presented. In Section IV, the proposed EKF-based vibrometry technique for the DPCA-SAR system is developed. In Section V, a refinement of the EKF-based vibrometry technique for noise immunity is introduced. In Section VI, simulations and results of the improved EKF-based vibrometry method are discussed. Finally, the conclusions of this paper are presented in Section VII.

II. SIGNAL MODEL FOR DISPLACED-PHASE-CENTER SYNTHETIC APERTURE RADAR

Fig. 2 shows the data-collection geometry of a DPCA-SAR operating in ping-pong mode [22]. The baseline, B , is defined as the along-track spacing between the fore-antenna and the aft-antenna on the collection platform. Conceptually, in a ping-pong mode, the fore-antenna collects data at a given location u^* , while the aft-antenna is OFF. The aft-antenna collects at the same location, u^* , while

the fore-antenna is OFF. The time delay between the data collection of the two antennas is $\tau_B = B/V_a$, where V_a is the average antenna speed. This process repeats for the duration of the entire synthetic aperture. In this model, clutter is defined as any other target illuminated in the ground scene. For a particular range line, the slow-time signal of the clutter collected by the fore-antenna can be written as

$$c_1(\tau) = \sum_i \bar{\sigma}_i \exp \left[-jk_y y_i \tau - j \frac{4\pi}{\lambda} r_i + j\phi_i \right] \quad (1)$$

where $\bar{\sigma}_i$, y_i , r_i , and ϕ_i are the average reflectance, azimuthal position, range, and initial phase of the i th scatterer, respectively. The wavelength and carrier frequency of the sent pulse are λ and f_c , respectively. The slow time is $\tau = u/V_a$, and k_y is a scaling parameter

$$k_y \approx \frac{4\pi f_c V_a}{c R_0 f_{\text{prf}}} \quad (2)$$

where c is the propagation speed of the sent pulse, R_0 is the distance from the scene center to the midaperture, and f_{prf} is the pulse-repetition frequency (PRF). Assuming that the ground clutter is static and since the aft-antenna is illuminating the ground scene from the same location as the fore-antenna, the clutter signal will remain constant at every collection point u^* throughout the entire synthetic aperture. Therefore, for the same given range line, the slow-time signal of the clutter collected by the aft-antenna is the same clutter signal collected by the fore-antenna with a known time delay, τ_B

$$\begin{aligned} c_2(\tau) &= c_1(\tau - \tau_B) \\ &= \sum_i \bar{\sigma}_i \exp \left[-jk_y y_i (\tau - \tau_B) - j \frac{4\pi}{\lambda} r_i + j\phi_i \right]. \end{aligned} \quad (3)$$

Now consider a single vibrating target at a given range line. The slow-time signal from a vibrating target collected by the fore-antenna is

$$d_1(\tau) = \bar{\sigma}_v \exp \left[-jk_y \bar{y}_v \tau - j \frac{4\pi}{\lambda} x_v(\tau) + j\phi_v \right] \quad (4)$$

where $\bar{\sigma}_v$, \bar{y}_v , and $x_v(\tau)$ are the average reflectance, average azimuthal position, and displacement of the vibrating target, respectively. Consequently, the slow-time signal from the vibrating target collected by the aft-antenna, $d_2(\tau)$, is

$$d_2(\tau) = \bar{\sigma}_v \exp \left[-jk_y \bar{y}_v (\tau - \tau_B) - j \frac{4\pi}{\lambda} x_v(\tau) + j\phi_v \right]. \quad (5)$$

The first phase term of $d_2(\tau)$ is $-jk_y \bar{y}_v (\tau - \tau_B)$, as shown in the case of clutter. However, the second phase term of $d_2(\tau)$ remains the same as that for $d_1(\tau)$ because the aft-antenna also observes the instantaneous vibration displacement $x_v(\tau)$ at time τ . In summary, the two slow-time signals collected by the fore-antenna and the aft-antenna, from a ground scene containing a single vibrating target in clutter, can be written as

$$s_1(\tau) = d_1(\tau) + c_1(\tau) + w_1(\tau) \quad (6)$$

and

$$s_2(\tau) = d_2(\tau) + c_2(\tau) + w_2(\tau) \quad (7)$$

where d_1 and d_2 represent the signals from the vibrating target, c_1 and c_2 represent the clutter signals, and w_1 and w_2 represent the additive noise due to electronic error and quantization error, etc. Just as in the signal model for spotlight SAR mode [12], w_1 and w_2 are modeled as zero-mean circularly symmetric complex-valued white Gaussian (ZMCSCG) noise.

Recall that the clutter signal collected by the fore-antenna is the same as the clutter signal collected by the aft-antenna separated by a time delay, τ_B , namely, $c_2(\tau) = c_1(\tau - \tau_B)$. Hence, by taking the difference of the signals collected by the two antennas at the same collection location u^* , the clutter signal is totally removed, and as a result, the difference signal is modulated by the vibration dynamics in a nonlinear manner. The difference signal, $s(\tau)$, which we call the DPCA signal of interest (SoI), is given by

$$s(\tau) = d_2(\tau + \tau_B) - d_1(\tau) + w_2(\tau + \tau_B) - w_1(\tau). \quad (8)$$

The operation represented by (8) is the DPCA technique [23]. In real-world applications, the removal of the clutter signal is subject to the noise floor of the DPCA-SAR system [23]. If we define the difference signal from the vibrating target as

$$d(\tau) = d_2(\tau + \tau_B) - d_1(\tau) \quad (9)$$

and the residual clutter noise as

$$w(\tau) = w_2(\tau + \tau_B) - w_1(\tau) \quad (10)$$

the DPCA-SAR SoI can be recast succinctly as

$$s(\tau) = d(\tau) + w(\tau). \quad (11)$$

In practice, the residual-clutter noise term may also include a portion of the clutter signal that is not canceled due to the incoherence between the signals collected by the fore- and the aft-antennas. For a typical DPCA-SAR collection platform, τ_B is no more than a few milliseconds. If τ_B is much shorter than the duration of the vibration of interest, then the instantaneous vibration displacement can be approximated linearly as

$$x_v(\tau + \tau_B) \approx x_v(\tau) + V_v(\tau)\tau_B \quad (12)$$

where $V_v(\tau)$ is the instantaneous vibration velocity. With this assumption, $d(\tau)$ can be expressed as

$$\begin{aligned} d(\tau) &\approx 2\sigma_v(\tau) \sin \left(\frac{2\pi \tau_B V_v(\tau)}{\lambda} \right) \\ &\times \exp \left[-j \frac{2\pi}{\lambda} (2x_v(\tau) + \tau_B V_v(\tau)) - j \frac{\pi}{2} \right] \end{aligned} \quad (13)$$

where

$$\sigma_v(\tau) = \bar{\sigma}_v \exp[-jk_y y_v \tau + j\phi_v]. \quad (14)$$

For a simple point target, the value of $\sigma_v(\tau)$ is simply the scaled pixel value in a complex SAR image, where $\bar{\sigma}_v$ corresponds to the pixel magnitude and ϕ_v corresponds to the pixel phase. The slow-time signal, $s(\tau)$, collected by the SAR platform is automatically sampled with the PRF. Therefore, the observed DPCA-SAR SoI can be written in discrete time as

$$s[n] = d[n] + w[n], \quad n = 1, \dots, N \quad (15)$$

and

$$d[n] = 2\sigma_v[n] \sin\left(\frac{2\pi\tau_B V_v[n]}{\lambda}\right) \times \exp\left[-j\frac{2\pi}{\lambda}(2x_v[n] + \tau_B V_v[n]) - j\frac{\pi}{2}\right] \quad (16)$$

where

$$\sigma_v[n] = \bar{\sigma}_v \exp[-jk_y y_v n + j\phi_v] \quad (17)$$

and N is the total number of the observed signal samples. The sampling interval, Δt , is the pulse-repetition interval (PRI) of the SAR system. The signal-to-noise ratio (SNR_{res}) of the DPCA-SAR SoI is defined as

$$\text{SNR}_{\text{res}} = 10 \log_{10} \left(\frac{\bar{\sigma}_v^2}{\sigma_w^2} \right) \quad (18)$$

where σ_w^2 is the variance of the residual clutter noise $w[n]$.

There are two major differences between the DPCA-SAR SoI shown in (15) and the SoI of a common SAR system (see [12, eq. (9)]). First, both the magnitude and phase of $d[n]$ in the DPCA-SAR SoI are nonlinearly modulated by the vibration dynamics. However, only the phase of $d[n]$ in the SAR SoI is linearly modulated by the vibration displacements. The DFrFT-based method is applicable only when the magnitude of $\tilde{d}[n]$ remains the same (or changes very slowly compared with the vibration) [12], [16], [24]. This is not the case for the DPCA-SAR SoI because the magnitude of $d[n]$ in the DPCA-SAR SoI changes as fast as the vibration velocity. Therefore, the DFrFT-based method is generally not applicable to the DPCA-SAR SoI. Second, the clutter signal is removed entirely from the DPCA-SAR SoI, while the SAR SoI suffers from the clutter signal. Because the DPCA-SAR SoI is only corrupted by additive noise as the clutter signal is removed, one can apply general signal estimation methods to the DPCA-SAR SoI for extracting $x_v[n]$ and $V_v[n]$. In this paper, these vibration dynamics are estimated from the DPCA-SAR SoI using a method based on the EKF. To achieve this, the EKF method must exploit the information contained in both the envelope and the phase of the DPCA-SAR SoI.

III. EXISTING VIBROMETRY TECHNIQUE FOR DISPLACED-PHASE-CENTER ANTENNA SYNTHETIC APERTURE RADAR

The robustness of DPCA-SAR in high clutter environments makes this radar configuration highly attractive for vibrometry applications. In the case when the vibration of the target is produced by a single-component sinusoidal function, the problem of estimating its frequency is relatively simple. In this case, the magnitude of the DPCA-SAR SoI can be used to estimate the vibration frequency. This is what we present below as the *magnitude method*. However, while this straightforward approach is simple, it is unlikely to be optimal because it utilizes only partial information (i.e., the envelope) of the DPCA-SAR SoI to conduct the estimation. Furthermore, this technique is not appropriate for complex vibrations.

A. Magnitude Vibrometry Method

From (16), the magnitude of $d[n]$ can be written as

$$|d[n]| = 2\bar{\sigma}_v \left| \sin\left(\frac{2\pi\tau_B}{\lambda} V_v[n]\right) \right|. \quad (19)$$

The instantaneous velocity $V_v[n]$ of a single-component vibration can be parameterized as

$$V_v[n] = M_v \cos(2\pi f_v \Delta t n + \psi_v) \quad (20)$$

where M_v is the magnitude of velocity, f_v is the frequency of the vibration, and ψ_v is the initial phase. We assume that

$$M_v \leq \frac{\lambda}{4\tau_B} \quad (21)$$

or equivalently

$$-\frac{\pi}{2} \leq \frac{2\pi\tau_B}{\lambda} V_v[n] \leq \frac{\pi}{2}. \quad (22)$$

In this case, there is a one-to-one mapping from $V_v[n]$ to $|d[n]|$ when $V_v[n] > 0$, and there is the same one-to-one mapping from $-V_v[n]$ to $|d[n]|$ when $V_v[n] < 0$. This implies that $|d[n]|$ repeats itself twice as fast as $V_v[n]$. As such, $|s[n]|$ also repeats itself twice as fast as $V_v[n]$ modulo the interference from the additive noise. Provided that the SNR_{res} is sufficiently high, f_v can be estimated as a half of the frequency of $|s[n]|$.

The magnitude of velocity of low-level vibrations is usually small. For instance, the magnitude of velocity of a 2-mm 10-Hz vibration is approximately 0.13 m/s. On the other hand, the upper bound, $\lambda/4\tau_B$, in the right-hand side of (21) is more than 1 m/s for typical SAR systems. Therefore, the constraint in (21) will be generally satisfied for the low-level vibrations of interest. In the extreme case where $M_v > \lambda/4\tau_B$, the mapping from $V_v[n]$ to $|d[n]|$, for either $V_v[n] > 0$ or $V_v[n] < 0$ cases, is no longer bijective. As a consequence, harmonic frequencies of f_v appear in the spectrum of $|d[n]|$ that cause ambiguity in estimating the vibration frequency.

The magnitude method is generally not applicable to multicomponent vibrations. For instance, we can write $|d[n]|$ for a two-component vibration as

$$|d[n]| = 2\bar{\sigma}_v |\sin(k_1 v_1[n] + k_2 v_2[n])| \quad (23)$$

or equivalently

$$|d[n]| = 2\bar{\sigma}_v |\sin(k_1 v_1[n]) \cos(k_2 v_2[n]) + \cos(k_1 v_1[n]) \sin(k_2 v_2[n])| \quad (24)$$

where k_1 and k_2 are known scalars, and $v_1[n]$ and $v_2[n]$ are the instantaneous velocities of the two vibrating components. According to (24), the relationship between the frequencies of $v_1[n]$ and $v_2[n]$, on the one hand, and the frequencies of $|d[n]|$ on the other hand, is not trivial; therefore, the magnitude method is not applicable in this case.

IV. PROPOSED VIBROMETRY METHOD BASED ON THE EXTENDED KALMAN FILTER

To overcome the shortcomings of the magnitude vibrometry method, an estimation tool, based on the EKF to estimate the vibration dynamics by exploiting the full information (both the envelope and the phase) of the DPCA-SAR SoI,

is presented. As it will be shown in the following sections, the EKF-based vibrometry technique is reliable not only for recovering single component vibrations from DPCA-SAR images but also for estimating complex vibrations (multicomponent and time varying) from DPCA-SAR images.

A. One-Step State-Transition Model

Using the previously presented DPCA-SAR signal model, it is possible to define a state vector as

$$\mathbf{X}_n = (x_v[n], V_v[n])^T \quad (25)$$

where n is each slow-time step. The state variables $x_v[n]$ and $V_v[n]$ are the instantaneous position and velocity, in the range direction, of the vibrating target, correspondingly. Let $A_v[n]$ denote the instantaneous acceleration of the vibrating target. Then, the one-step state-transition model can be written as

$$\mathbf{X}_{n+1} = \mathbf{F}\mathbf{X}_n + \mathbf{G}A_v[n] \quad (26)$$

where

$$\mathbf{F} = \begin{pmatrix} 1 & \tau_B \\ 0 & 1 \end{pmatrix} \quad (27)$$

and

$$\mathbf{G} = (0, \tau_B)^T. \quad (28)$$

Consistent with the EKF setting, we assume $A_v[n]$ to be a zero-mean white Gaussian process; this assumption is justified in the next paragraph. Note that the state-transition model (26) does not make any assumptions about the vibration behavior of the vibrating target other than that it must obey Newton's laws of motion. Therefore, this model applies for complex vibrations that increase or decrease in frequency during the collection process.

We now justify the assumption on $A_v[n]$ using, for simplicity, a single-component sinusoidal vibration. Note that the acceleration signal, $A_v(\tau)$, in this case is of the form

$$A_v(\tau) = A_d(2\pi f_v)^2 \cos(\omega_0 \tau + \Theta) \quad (29)$$

where $\omega_0 = 2\pi f_v$, with f_v being a uniform random variable in $[0, f_{\text{prf}}/2]$, Θ is a uniform random variable in $[-\pi, \pi]$, and A_d is a uniform random variable in $[0, d_{\text{max}}]$, with d_{max} being the maximum amplitude of a measurable displacement. The random variables f_v , Θ , and A_d are assumed to be independent. Next, it can be shown that the auto-covariance function of $A_v(\tau)$ is given by

$$R_{A_v A_v}(\tau) = \frac{d_{\text{max}}^2 (\pi f_{\text{prf}})^3 \sin(\pi f_{\text{prf}} \tau)}{30 \tau}. \quad (30)$$

Therefore, since the sampling time is given by the PRI, and $\tau = n\Delta t = n/f_{\text{prf}}$, (30) becomes a delta function. Thus, it is not unreasonable to consider $A_v[n]$ as a zero-mean white Gaussian process for a sinusoidal acceleration in the one-step state-transition model (26). Note, however, if the range of f_v is not $[0, f_{\text{prf}}/2]$, then (30) will approximate a delta function.

B. Observation Model

For the DPCA-SAR system and the previous one-step state-transition model, the observation model is given by

$$\begin{aligned} s[n] &= d[n] + w[n] \\ &\equiv h(\mathbf{X}_n) + w[n]. \end{aligned} \quad (31)$$

From (16), it is clear that $d[n]$ (and therefore the observation model) is nonlinear with respect to the state vector \mathbf{X} . In the EKF, the observation matrix \mathbf{H}_n is defined as

$$\mathbf{H}_n = \nabla h |_{\mathbf{X}=\hat{\mathbf{X}}_{n|n-1}} \quad (32)$$

where $\hat{\mathbf{X}}_{n-1}$ is the estimation of \mathbf{X}_{n-1} . As such, the linearized observation model can be written as

$$s[n] = \mathbf{H}_n \mathbf{X}_n + w[n] \quad (33)$$

where

$$\begin{aligned} \mathbf{H}_n &= (4\kappa \bar{\sigma}_v \sin(\kappa \tau_B \hat{\mathbf{X}}_{n-1}(2)) e^{j\Phi_n - j\pi/2}, \\ &\quad 2\kappa \tau_B \bar{\sigma}_v \cos(\kappa \tau_B \hat{\mathbf{X}}_{n-1}(2)) e^{j\Phi_n} \\ &\quad - 2\kappa \tau_B \bar{\sigma}_v \sin(\kappa \tau_B \hat{\mathbf{X}}_{n-1}(2)) e^{j\Phi_n - j\pi/2}) \end{aligned} \quad (34)$$

$$\kappa = \frac{2\pi}{\lambda} \quad (35)$$

and

$$\begin{aligned} \Phi_n &= -k_y y_v n \Delta t + \phi_v \\ &\quad - \frac{2\pi}{\lambda} \left(2\hat{\mathbf{X}}_{n-1}(1) + \tau_B \hat{\mathbf{X}}_{n-1}(2) \right) - \frac{\pi}{2}. \end{aligned} \quad (36)$$

In our formulation, it is assumed that the variance of the noise $w[n]$ is known. With the one-step state-transition model given in (26) and the linearized observation model given in (33), the Kalman filter described in [25] and [26] can be used to estimate the vibration dynamics with an initial condition. The solution to the vibration-estimation problem using the Kalman filter is given as follows. We begin by defining

$$s_i^j = (s[i], \dots, s[j])^T, \quad i < j \text{ and } 0 \leq i, j \leq N. \quad (37)$$

Next, let $\hat{\mathbf{X}}_{n+1|n}$ and $\hat{\mathbf{X}}_{n|n}$ be the predicted and corrected state estimates, respectively. Then, the state estimates $\hat{\mathbf{X}}_{n+1|n} \doteq E[\mathbf{X}_{n+1} | s_0^n]$ and $\hat{\mathbf{X}}_{n|n} \doteq E[\mathbf{X}_n | s_0^n]$ are given recursively by

$$\hat{\mathbf{X}}_{n+1|n} = \mathbf{F}\hat{\mathbf{X}}_{n|n}, \quad n = 1, 2, \dots \quad (38)$$

and

$$\hat{\mathbf{X}}_{n|n} = \hat{\mathbf{X}}_{n|n-1} + \mathbf{K}_n (s[n] - \mathbf{H}_n \hat{\mathbf{X}}_{n|n-1}), \quad n = 1, 2, \dots, \quad (39)$$

with the initialization $\hat{\mathbf{X}}_{0|-1} = E[X_0]$. (Here, $E[U]$ is the expected value of the random variable U , and $E[U|Z]$ is the conditional expectation of the random variable U given the random variable Z .) In this paper, it is assumed that any vibrating target has symmetrical displacements and velocities with respect its central position. Therefore, $\hat{\mathbf{X}}_{0|-1} = E[X_0] = 0$. The Kalman gain, \mathbf{K}_n , is given by

$$\mathbf{K}_n = \Sigma_{n|n-1} \mathbf{H}_n^T (\mathbf{H}_n \Sigma_{n|n-1} \mathbf{H}_n^T + \sigma_w^2)^{-1} \quad (40)$$

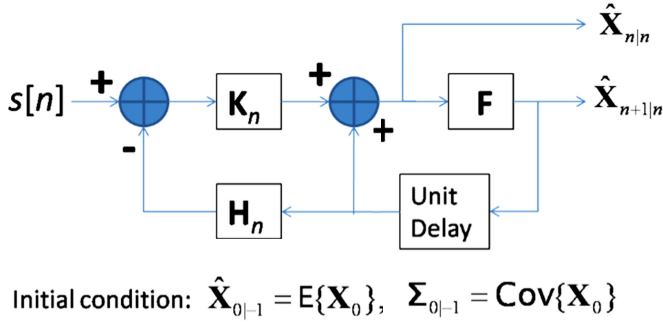


Fig. 3. Block diagram of the Kalman filter for vibration estimation in DPCA-SAR. The variable $s[n]$ is the DPCA-SAR SoI, \mathbf{K}_n is the Kalman gain, \mathbf{H}_n is the linearized observation matrix, and \mathbf{F} is the one-step state-transition matrix.

where $\Sigma_{n|n-1} \doteq \text{Cov}(X_n | s_0^{n-1})$ and \mathbf{H}_n^T is the transpose of \mathbf{H}_n . The covariance matrix, $\Sigma_{n|n-1}$, can be computed jointly with $\Sigma_{n|n} \doteq \text{Cov}(X_n | s_0^n)$ from the following recursion:

$$\Sigma_{n|n} = \Sigma_{n|n-1} + \mathbf{K}_n \mathbf{H}_n \Sigma_{n|n-1}, \quad n = 1, 2, \dots \quad (41)$$

and

$$\Sigma_{n+1|n} = \mathbf{F} \Sigma_{n|n} + \mathbf{F}^T \mathbf{G} \mathbf{Q}_n \mathbf{H}^T, \quad n = 1, 2, \dots \quad (42)$$

with the initialization $\Sigma_{0|0} \doteq \text{Cov}(X_0)$, where \mathbf{Q}_n is the covariance matrix of the instantaneous vibration acceleration $A_v[n]$. Fig. 3 shows the block diagram of the Kalman filter for the vibration estimation problem.

V. OBSERVATION NOISE IMMUNITY BY AVERAGING OVER SEVERAL STATE ESTIMATES

A. Motivation

Recall that when the state-transition model was defined, no assumptions were made about the vibration behavior of the vibrating target other than it was obeying the classical laws of motion. Defining the state-transition model in this manner permits the vibration dynamics of the vibrating target to change drastically between each slow-time step. However, while it is not constrained in the state-transition model, it was assumed that the PRI was significantly shorter than the period of the vibration of interest. With this assumption, it is not physically possible for the vibrating target to exhibit a drastic change of position between each slow-time step. Therefore, any nontrivial changes in the vibration dynamics of the vibrating target in the observed signal, $s[n]$, between successive slow time steps, are caused solely by the observation noise. Since the state-transition model does not account for this and since the observations are linearized at each slow-time step, the standard implementation of the EKF is very susceptible to observation noise. This susceptibility to noise can lead to incorrect state-variable estimates and misleading vibration behavior. If the observation noise is suppressed, the EKF becomes much more accurate and stable.

It is widely known that the state estimates of the EKF may diverge when the error covariance becomes significantly small. In fact, some variations of the EKF have been developed for compensating the uncertainties in the error covariance

introduced by the first-order linearization. One of the most popular is the unscented Kalman filter (UKF) [27], [28]. The UKF was originally developed under the idea that the linearization step of the EKF can produce a highly unstable filter if the assumptions of local linearity are violated. Specifically, the UKF employs an unscented transformation to estimate the statistics of the state variables as they pass through the nonlinear system. In this way, the UKF produces estimates of third-order accuracy while the EKF produces estimates of first-order accuracy [28]. In contrast, in this paper, we present a special modification to the EKF in order to reduce the adverse effect of severe data variability on the piecewise-linear assumption. Specifically, in this paper, we average the state estimates to produce more stable estimates, which, in turn, is used in the computation of the linearized observation matrix.

To motivate this averaging approach, consider the case of a single static target. Each time the static target is observed, the observation noise randomly places the target at the incorrect position in the ground scene. If the static target is repeatedly observed over an extended period of time, each observation will create a set of different possible target locations. This set of all observations will be a scattering of locations, centralized and symmetric around the true target location. The centralized and symmetric scattering of observations is because the noise is assumed to be ZMCSCG. As the number of observations increases, the expected value of the set of all the observations will approach the true target location. Thus, resilience to noise is directly related to the number of averaged state estimates. However, in this article, all the targets of interest are vibrating. Thus, averaging over too many state estimates while suppressing the noise will also suppress the vibration behavior and only the average target position will remain. Therefore, it is critical to average over as many state estimates as possible to suppress the noise, while not averaging over too many state estimates to ensure retention of the vibration behavior of the target. An analytical expression to determine the number of points to average over is developed below.

If f_v is the vibration frequency of the target of interest, then $1/f_v$ is the time needed for a single complete vibration cycle, or period, M is the number of averaged points for noise suppression, and Δt is the PRI. Then, the state estimates are being averaged over the time interval, $M \Delta t$. Taking the ratio of these quantities gives the ratio of a single vibration that the state estimates are estimated over

$$\frac{M \Delta t}{\frac{1}{f_v}} = \beta. \quad (43)$$

Setting $\beta \approx 0.125$ ensures that the average is taken over at most 1/8 of the vibrating period. Averaging over 1/8 or less of the vibrating period appears to ensure the vibration dynamics are not substantially suppressed. As can be seen in Section VI, this rule holds for many different target dynamics: sinusoidal and stationary vibrations, sinusoidal and linearly increasing in frequency vibrations, and multicomponent sinusoidal vibrations. While any $\beta \leq 0.125$ is sufficient to retain the vibration behavior, increasing the time of the averaging will increase the

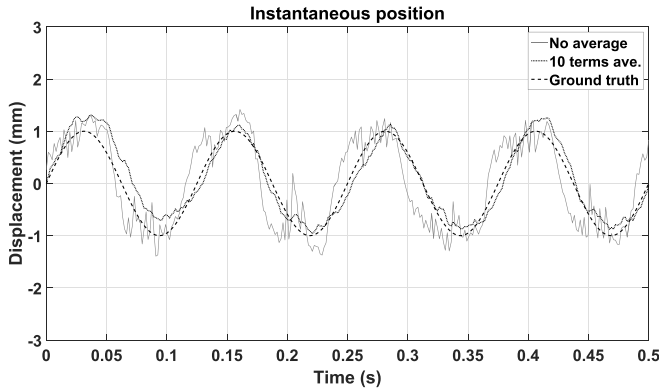


Fig. 4. Estimated position of a 1-mm 8-Hz vibrating target using the EKF. The DPCA-SAR SoI was contaminated with ZMCSCG noise with an SNR_{res} of 15 dB. State-estimate averaging improves the estimated position of the vibrating target significantly when using the EKF-based method. In this example, the MSE is reduced by 34%.

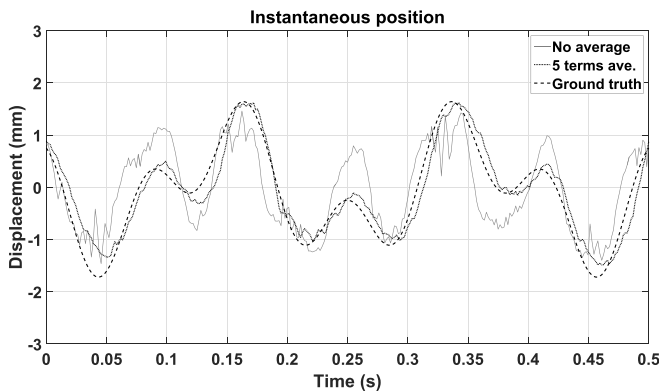


Fig. 5. Estimated position of a multicomponent vibration. The components are 1 mm, 5 Hz and 0.75 mm and 12 Hz. The DPCA-SAR SoI was contaminated with ZMCSCG noise with an SNR_{res} of 15 dB. State-estimate averaging improves the estimated position of the vibrating target significantly when using the EKF-based method. In this example, the MSE is reduced by 76%.

noise immunity. Therefore, M should be as large as possible, while ensuring $\beta \approx 0.125$. This condition can be expressed mathematically as

$$M = \max \left\{ n \in \mathbb{N} : n \leq \frac{0.125}{\Delta t f_v} \right\}. \quad (44)$$

Note that for a given vibration frequency, as the PRF increases (i.e., Δt decreases), the number of state estimates that can be averaged, M , increases. Therefore, for a given target vibration frequency and SNR_{res} value, a higher PRF (low Δt) increases noise immunity. This is further discussed in Section V-D and Fig. 7. An example of the improvement obtained using the state-estimate averaging is shown in Figs. 4 and 5. As can be seen in Figs. 4 and 5, the averaging technique drastically improves the resemblance of the estimated instantaneous position of the target with the ground truth. The introduction of the state-estimate averaging method to the EKF is presented in Section V-C.

B. Determining an Approximate f_v A Priori

One of the potential stumbling blocks of the state-estimate-averaging method is that it depends on having some prior knowledge of the vibration frequency of the target of interest. However, this is not an entirely unreasonable assumption. The vibration dynamics of a target are dependent on the material, geometry, and the machinery that is generating the vibrations. For example, if a corporation does remote monitoring of its own systems, it will have access to the material, geometry, and the machinery that is generating the vibrations. Therefore, a range of expected vibration frequencies will be known. If $f_{\text{max}(v)}$ is the maximum expected vibration frequency of a given target, then (44) can be restated as

$$M = \max \left\{ n \in \mathbb{N} : n \leq \frac{0.125}{\Delta t f_{\text{max}(v)}} \right\}. \quad (45)$$

In other scenarios, the geometry, material, and machinery can be determined with other remote sensing techniques such as optical, infrared, and multispectral, to name a few. Therefore, in most cases, a maximum expected vibration frequency, $f_{\text{max}(v)}$, can be estimated.

C. Refinement of the EKF for Increased Noise Immunity

Since it is the effect of the observation noise in the EKF model, rather than system noise, that is being mitigated with the state-estimate averaging described in Section V-A, the state-transition model, as defined in (26), remains unchanged as this is an accurate description for the vibration behavior. Any changes to the state-transition model in an attempt to gain noise immunity would lead to an incorrect state model. In addition, the observation model defined in (31) remains unchanged as the DPCA-SAR collection platform has a fixed imaging procedure that cannot be altered. The modification occurs in the linearization of the observation model, as it is the linearization that is susceptible to the observation noise.

Let N_1 be the total number of state estimates being averaged, where N_1 is determined by (44). Then, the observation matrix, \mathbf{H}_n , is now defined as

$$\mathbf{H}_n = \nabla h \big|_{\mathbf{x}=\hat{\mathbf{x}}_{\text{avg}(n)}} \quad (46)$$

where

$$\hat{\mathbf{x}}_{\text{avg}(n)} = \frac{\hat{\mathbf{x}}_{n|n-1} + \hat{\mathbf{x}}_{n-1|n-2} + \cdots + \hat{\mathbf{x}}_{n-N_1+1|n-N_1}}{N_1}. \quad (47)$$

Here, the initialization of the state estimates is given by

$$\hat{\mathbf{x}}_{N_1-1|N_1-2} = \cdots = \hat{\mathbf{x}}_{1|0} = \hat{\mathbf{x}}_{0|-1} = E[X_0] = 0. \quad (48)$$

This is the sole place in the EKF algorithm at which state estimates averaging is used to provide noise immunity. The rest of the EKF algorithm remains as defined from (33) to (42).

D. Noise Requirements

One of the potential challenges when implementing the EKF is that under certain conditions, the state estimations provided through the EKF algorithm can diverge from the

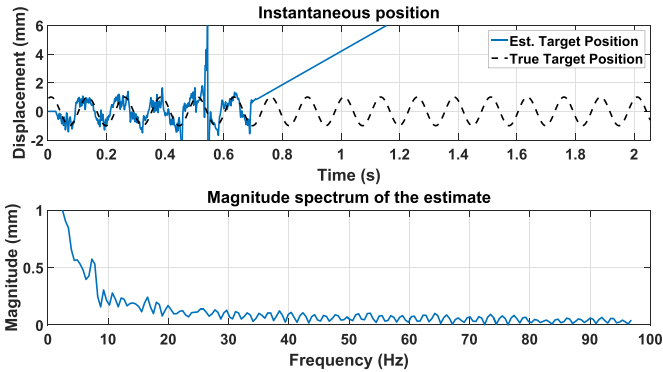


Fig. 6. Estimated position and estimated frequency of a 1-mm 8-Hz vibrating target using the EKF. The DPCA-SAR SoI was contaminated with ZMCSCG noise with an SNR_{res} of 9 dB. Strong successive noisy observations cause the Kalman gain to place unreasonable trust in the predicted state estimates and not trust the observations.

TABLE I
PERFORMANCE LIMITS OF DPCA-SAR VIBRATION ESTIMATION USING THE EKF METHOD

Parameter	Quantity
Required SNR_{res} :	15 dB
Frequency Resolution:	$\frac{1}{f_{\text{prf}} N}$
Maximum measurable vibration velocity (MMVV):	$\frac{\lambda}{4\tau_B}$
Maximum measurable vibration frequency (MMVF):	theoretically $\frac{f_{\text{prf}}}{2}$; with state averaging $\frac{f_{\text{prf}}}{2N_1}$

actual state variables. This divergence is typically caused by the trace of the error covariance matrix becoming extremely small. When the trace of the covariance matrix is very close to zero, the Kalman gain places unreasonable trust in the state prediction and ignores subsequent observations [29]. When this occurs, the vibrational dynamics of targets cannot be reliably determined. Therefore, for accurate vibrometry, it is necessary to characterize the pervasiveness of this divergence and to determine how to reduce the divergence to negligible levels.

An example of what happens to the state estimate when the estimated state-error-covariance matrix becomes unrealistically small is shown in Fig. 6. It is clear that EKF no longer trusts the observations and the state estimates are updated only using the predictions from the state-transition model.

For the purpose of characterizing the reliability of the EKF against residual clutter noise, the vibrating target is assumed to have a steady (constant frequency) sinusoidal motion of 8 Hz with a 1-mm displacement. The system parameters used for this characterization are described in Table II. With these target dynamics, 1000 simulated slow-time DPCA-SAR SoIs were generated. Each realization of the slow-time signal was corrupted with a ZMCSCG perturbation as residual clutter noise. Then, the previously developed EKF-vibrometry method was applied to each slow-time signal. If the EKF-

TABLE II
DPCA-SAR SYSTEM PARAMETERS USED IN SIMULATIONS

Parameter	Quantity
Center frequency	16 GHz
Effective PRF	487 Hz
Propagation velocity	3×10^8 m/s
Platform velocity	175 m/s
Slant range	10 km
Azimuth resolution	0.33 m
Aperture length	363 m
SNR_{res}	15 dB
Baseline	0.3596 m

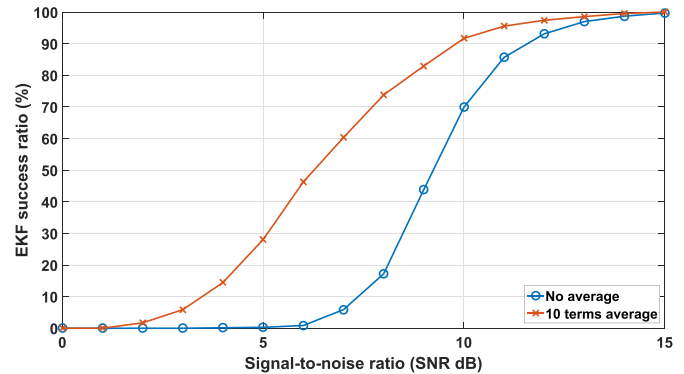


Fig. 7. Percentage of reliability in estimating the frequency of the vibrating target within 1 Hz over 1000 SoI for a given residual SNR_{res} value. The vibrating target had a frequency of 8 Hz and a magnitude of 1 mm. As can be observed, the proposed averaging technique drastically improves the reliability of the EKF when $3 \text{ dB} \leq \text{SNR}_{\text{res}} \leq 11 \text{ dB}$.

vibrometry method estimated the frequency of the vibrating target within an error margin of 1 Hz, then the estimation was considered to be reliable or to have converged; otherwise, the method was considered to have produced an unreliable estimate or have diverged. The ratio of converging solutions to the total number of slow-time SoI was taken as a reliability indicator. This process was repeated for integer SNR_{res} values ranging from 1 to 15 dB. This entire procedure was done with the averaging for noise immunity method and without the averaging for noise immunity method. The results are shown in Fig. 7. As can be observed, for a given level of residual SNR_{res} , the state-estimate averaging for noise immunity increases the occurrence of converging solutions. For example, when the SNR_{res} is 8 dB, the percentage of diverging solutions is approximately reduced from 80% to 25% when employing the state-estimate-averaging technique. Therefore, for the minimal computational effort, averaging provides not only increased confidence in the vibration behavior but also decreases the likelihood of a divergent solution when the residual clutter noise exhibits $\text{SNR}_{\text{res}} < 15 \text{ dB}$. When the SNR_{res} exceeds 15 dB, the divergence of the estimates is no longer a concern. In fact, the $\text{SNR}_{\text{res}} \geq 15 \text{ dB}$ requirement is quite reasonable since values between 15 and 20 dB of SNR_{res} are typical thresholds for target detection in MTI systems [30]. The performance limits of the proposed method are summarized in Table I.

E. Signal-to-Clutter Ratio

In a general sense, clutter can be defined as the collection of all targets or objects that engender undesired reflections in the returned radar signal. These undesired reflections often degrade the performance of the radar system as the target of interest cannot be separated from the background. Clutter can be placed into one of two categories: surface clutter and airborne clutter. Some examples of surface clutter include vegetation, ground terrain, ocean surface condition, and jungle canopies. Airborne clutter, sometimes termed volume clutter, typically refers to rain, insects, or birds. In this paper, only ground clutter is considered. Since a SAR is designed to be an all-weather imaging system, the majority of airborne clutter typically has minimal, and often negligible, effects on the quality of the SAR image [31]–[33].

One of the distinct advantages of a DPCA-SAR system is that it performs quite well when introduced into a high clutter environment. In real-world applications, the removal of the clutter signal is subject to the noise floor of the DPCA-SAR system [23]. When the noise increases, residual clutter (from imperfect noise cancellation) will be present. However, this residual clutter will be indistinguishable from the noise signal. This noise is generated from any incoherence between the two antennas, in addition to the thermal noise [34]. This incoherence is generated from a variety of imperfections in the collection platform, as well as natural background radiation.

One source that produces the stated incoherence is imperfections in the flight path due to turbulence. An irregular flight path causes the aft-antenna to be in a slightly different collection location than the fore-antenna. As a consequence, the DPCA-SAR system is not capable of producing a perfect cancellation due to the differences in the clutter signals collected by the two antennas. Typically on board a SAR platform, there is a GPS as well as some type of inertial measurement unit (IMU) or guidance system. These systems track the position of the collection platform for the duration of the flight. The GPS and IMU typically help to compensate for the irregular flight path; however, their success is limited by their own error margins [35]. Since turbulence can be viewed as a random process and the GPS and IMU errors are random, this incoherence can be viewed as noise.

A second source that causes incoherence is the inconsistency between the fore- and aft-antennas. Any misalignment in phase results in a corresponding range error. With the same clutter signal mapped to a different range line for each antenna, these clutter signals will not be removed in the DPCA-SAR SoI. Since this phase error is due to real-world system limitations, it is random and can also be viewed as noise.

Therefore, even using adaptive correction techniques, as a practical matter, the clutter can only be canceled down to the noise level. Hence, the DPCA-SAR signal to residual-clutter ratio (SCR_{res}) is for all intents and purposes equivalent to the SNR_{res} . For vibrometry purposes, the effect of the residual clutter on the DPCA-SAR signal may be worse than the effect of the noise. However, the effect of the residual clutter cannot be less significant than the effect of the noise.

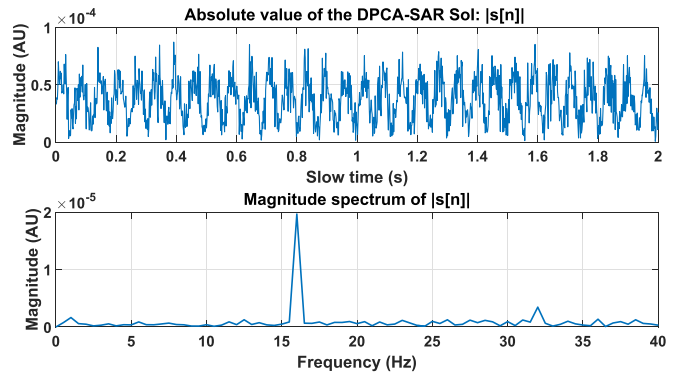


Fig. 8. Absolute value of the DPCA-SAR SoI and its frequency spectrum for a 1-mm 8-Hz vibrating target. The DPCA-SAR SoI was contaminated with ZMCSCG noise with an SNR_{res} of 15 dB. The vibration frequency can be estimated directly from the spectrum of the DPCA-SAR SoI. In this case, the 16-Hz peak indicates that the vibration frequency is 8 Hz.

VI. SIMULATIONS AND RESULTS

The presented EKF method has the ability to estimate not only the vibration frequency, but can also determine the instantaneous position and velocity of the vibrating target during the collection process. Since the EKF method is not restricted to a single-component sinusoidal vibration, it can be used to recover complex vibration, including multicomponent sinusoidal vibrations and vibrations with time-varying characteristics. In this section, the EKF-based vibrometry technique is tested for different vibration dynamics. Specifically, the vibration dynamics considered are a single-component sinusoidal vibration, a linearly increasing (and decreasing) frequency sinusoidal vibration, and a multicomponent sinusoidal vibration. For the case of a single-component sinusoidal vibration, the results of the magnitude method are presented for comparison. The vibrometry methods are validated by simulating the DPCA-SAR SoI, as described by (16). It is important to remember that the ground clutter present in the SAR images (captured by both the aft- and the fore-antennas) has been already suppressed in the DPCA-SAR SoI. However, we do consider residual clutter noise clutter/noise in the following simulations.

The simulated DPCA-SAR system is operating in the K_u -band and the corresponding system parameters are listed in Table II. These system parameters are chosen in part to mimic the Lynx radar [2]. The baseline, B , and the platform velocity, V_a , are, however, typical values of a DPCA-SAR system.

A. Simple Sinusoidal Vibration Simulation

The first set of simulations considers a vibrating target whose displacement is described through a sinusoidal vibration of constant frequency and constant amplitude. The target had an 8-Hz oscillation with an amplitude of 1 mm (i.e., a velocity of 50.26 mm/s). Figs. 8 and 9 show the results of applying the magnitude method for estimating the instantaneous velocity of the target. As can be observed in Fig. 8, the vibration frequency is contained in the spectrum of the DPCA-SAR

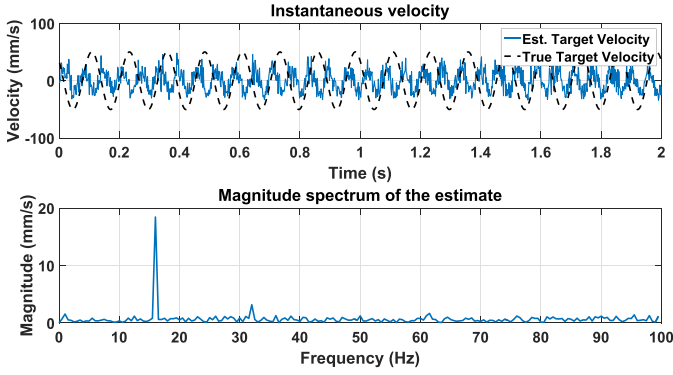


Fig. 9. Estimated velocity and estimated frequency spectrum of a 1-mm 8-Hz vibrating target using the magnitude method. The DPCA-SAR SoI was contaminated with ZMCSCG noise with an SNR_{res} of 15 dB. The recovered waveform exhibits a frequency component of twice the value of the original vibration.

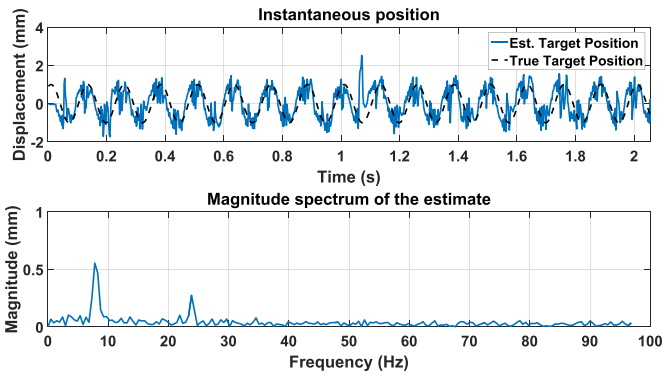


Fig. 10. Estimated position and estimated frequency spectrum of a 1-mm 8-Hz vibrating target using the EKF. The DPCA-SAR SoI was contaminated with ZMCSCG noise with an SNR_{res} of 15 dB.

SoI at the double of the original frequency (i.e., a 16-Hz component can be observed). Fig. 9 shows the velocity waveform recovered by solving (19). As can be observed, the recovered waveform exhibits the double of the frequency of the original signal due to the effect of the absolute value in (19). Meanwhile, Fig. 10 shows the results of the EKF-vibrometry method estimating the position of a vibrating target without using the state-estimate-averaging technique described in Section V. As can be observed in Fig. 10, the waveform recovered by the EKF-vibrometry method is highly affected by the residual clutter noise. This issue is addressed by applying the proposed state-estimate averaging, as shown in Fig. 11. In this case, the state-estimate averaging occurred over 10 consecutive terms. It is clear from Fig. 11 that the state-estimate average improves the position estimate of the vibrating target and, consequently, produces a sharper peak in the frequency spectrum of the estimated signal. In fact, when analyzing the mean square error (MSE) of the estimated position of the target, the first EKF method produces an MSE of 0.2279 mm^2 while the MSE of the modified method is 0.1503 mm^2 . Therefore, the modification improved the position estimate of the vibrating target by 34%. Finally, it should be noted that even though the magnitude method performs

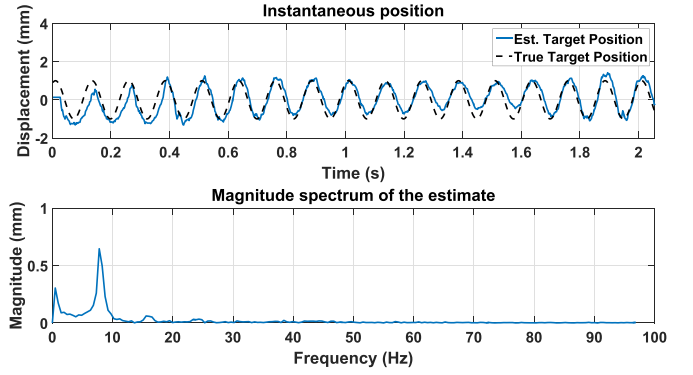


Fig. 11. Estimated position and estimated frequency spectrum of a 1-mm 8-Hz vibrating target using the EKF. The DPCA-SAR SoI was contaminated with ZMCSCG noise with an SNR_{res} of 15 dB. The state estimates were linearized over seven terms for noise suppression.

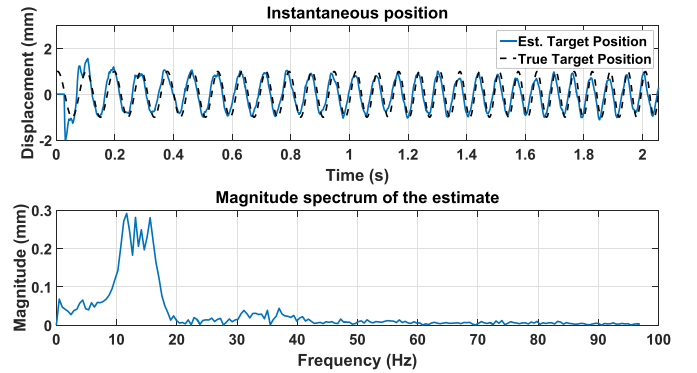


Fig. 12. Position estimation of a vibrating target with time-varying dynamics using the EKF. The vibration frequency linearly increased from 10 to 17 Hz. The amplitude of the vibration was 1 mm. The DPCA-SAR SoI was contaminated with ZMCSCG noise with an SNR_{res} of 15 dB. The state estimates were linearized over 10 terms for noise suppression.

well for a simple sinusoidal vibration, the algebraic solution becomes nontrivial as the vibration waveform increases in complexity as is explained in Section III-A. Therefore, the study cases shown next will not include this technique.

B. Sinusoidal Vibration With Linearly Increasing Frequency

The next simulation considers the case of a vibrating target whose displacement is described through a sinusoidal vibration that linearly increases in frequency throughout the duration of the aperture. The target oscillations started at 10 Hz and linearly increased to 17 Hz. The displacement of the vibrating target was set to 1 mm. The position estimate for the linear increasing vibration using the modified-EKF is shown in Fig. 12. As in the previous case of a constant frequency sinusoidal vibration, after about two complete oscillations, the estimated target position converges to the true target position.

C. Sinusoidal Vibration With Linearly Decreasing Frequency

In this case, we consider a vibrating target whose displacement is described through a sinusoidal vibration that linearly decreases in frequency throughout the duration of the aperture.

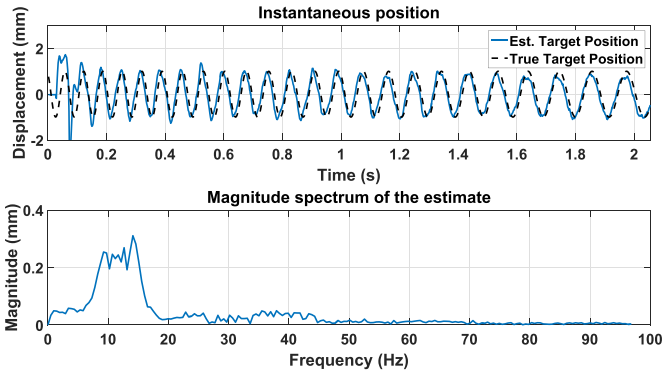


Fig. 13. Position estimation of a vibrating target with time-varying dynamics using the EKF. The vibration frequency linearly decreased from 16 to 8 Hz. The amplitude of the vibration was 1 mm. The DPCA-SAR SoI was contaminated with ZMCSCG noise with an SNR_{res} of 15 dB. The state estimates were linearized over 10 terms for noise suppression.

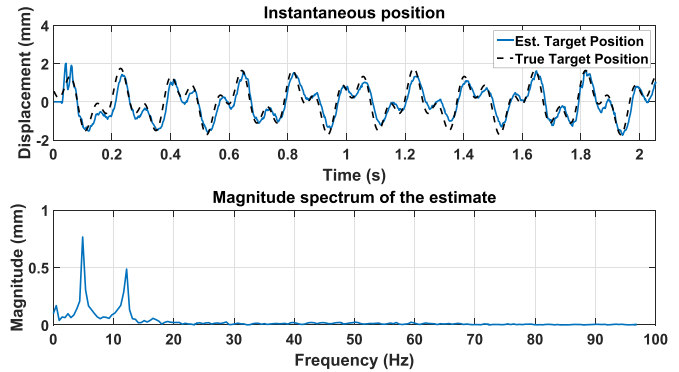


Fig. 15. Position estimation of a vibrating target that exhibits a multicomponent vibration using the EKF. Five state estimate terms were averaged. The vibration frequencies are 5 and 12 Hz, and the vibration amplitudes are 1 and 0.75 mm, respectively. The DPCA-SAR SoI was contaminated with ZMCSCG noise with an SNR_{res} of 15 dB.

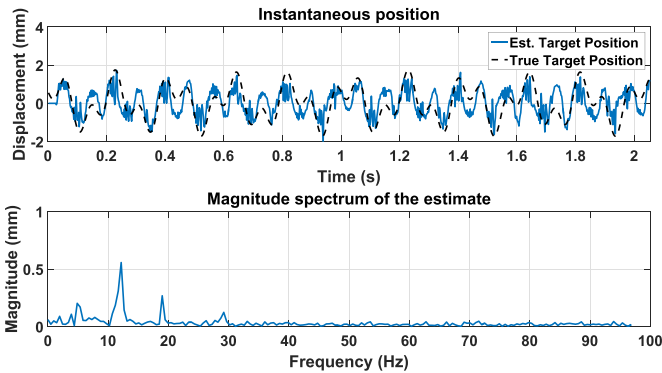


Fig. 14. Position estimation of a vibrating target that exhibits a multicomponent vibration using the EKF. No average of state estimates was employed. The vibration frequencies are 5 and 12 Hz, and the vibration amplitudes are 1 and 0.75 mm, respectively. The DPCA-SAR SoI was contaminated with ZMCSCG noise with an SNR_{res} of 15 dB.

The target oscillations started at 16 Hz and linearly decreased to 8 Hz. The displacement of the vibrating target was set to 1 mm. The position estimation for the linear increasing vibration using the modified-EKF is shown in Fig. 13. Similar to the previous cases, after approximately two oscillations, the estimated position of the vibrating target converges to the true target position.

D. Multicomponent Vibration

Finally, we considered the case of a vibrating target whose displacement is described as the sum of two sinusoids. The first frequency component has a 5-Hz vibration frequency with a displacement of 1 mm. The second frequency component has a 12-Hz vibration frequency with a displacement of 0.75 mm. The position estimation for the multicomponent vibration without state-estimate averaging is shown in Fig. 14. The position estimation for the multicomponent vibration with state-estimate averaging is shown in Fig. 15. As can be observed in Fig. 15, the state-estimate-averaging technique is required for accurately estimating the position of the vibrating target. Even with the additional vibration component, the estimated position closely matches the true target position. Since the

highest frequency component is 12 Hz, the state estimates are averaged over five consecutive terms. For this scenario, the modification of the EKF reduced the MSE of the estimated target position by 76%.

VII. CONCLUSION

In this paper, a novel vibrometry technique for a DPCA-SAR was presented. In contrast with the traditional SAR-vibrometry, the proposed vibrometry technique takes advantages of the DPCA-SAR signal model to remove all the ground clutter by combining two SAR images. Therefore, the proposed vibrometry technique can potentially recover the vibration dynamics of a vibrating target in the presence of heavy clutter. Specifically, the proposed vibrometry technique employs an EKF for estimating the instantaneous position and velocity of a target from a difference DPCA-SAR image. Since this technique does not impose specific requirements on the dynamics of the vibrations exhibited by a target, it can be used to estimate complex vibrations such as multicomponent sinusoidal vibrations and others with time-varying characteristics such as increasing (and decreasing) chirped sinusoidal vibrations. Furthermore, it has been demonstrated that the implementation of a state-estimate-averaging technique in the linearization step of the observation function of the EKF algorithm produces a profound positive impact on the performance of the vibrometry technique. In fact, the modification to the EKF presented in this paper improves the position estimate of the vibrating target by 34% when the SNR_{res} is 15 dB for a single-component vibrating target. For the multicomponent vibrations, the MSE of the estimated target position is reduced by 76% when the SNR_{res} is 15 dB. Moreover, the state-estimate-averaging technique augmented the reliability of the estimates and decreased the likelihood of divergence of the EKF solution for the position of the vibrating target. When the SNR_{res} is 8 dB, the percentage of diverging solutions is approximately reduced from 80% to 25% when employing the state-estimate-averaging technique. The next step for this vibrometry technique is to collect and analyze airborne data relevant to operational SAR systems such as, for example, the Lynx SAR.

ACKNOWLEDGMENT

The authors would like to thank General Atomics Aeronautical Systems, Inc. (San Diego, CA, USA) for making the Lynx system available for this paper.

REFERENCES

- [1] A. W. Doerry and F. M. Dickey, "Synthetic aperture radar," *Opt. Photon. News*, vol. 15, no. 11, pp. 28–33, Nov. 2004. [Online]. Available: <http://www.osa-opn.org/abstract.cfm?URI=opn-15-11-28>
- [2] S. I. Tsunoda *et al.*, "Lynx: A high-resolution synthetic aperture radar," *Proc. SPIE*, vol. 3704, pp. 20–27, Jul. 1999. [Online]. Available: <http://dx.doi.org/10.1117/12.354602>, doi: 10.1117/12.354602.
- [3] S. Chiu, "An analysis of RADARSAT2 SAR-GMTI performance for standard beam mode," Defence Res. Establishment, Ottawa, ON, Canada, Tech. Rep. DREOTR 2000-088, Dec. 2000. [Online]. Available: <http://www.dtic.mil/get-tr-doc/pdf?AD=ADA385571&Location=U2&doc=GetTRDoc.pdf>
- [4] R. K. Raney, "Synthetic aperture imaging radar and moving targets," *IEEE Trans. Aerosp. Electron. Syst.*, vol. AES-7, no. 3, pp. 499–505, May 1971.
- [5] T. Sparr and B. Krane, "Micro-Doppler analysis of vibrating targets in SAR," *IEE Proc.-Radar, Sonar Navigat.*, vol. 150, no. 4, pp. 277–283, Aug. 2003.
- [6] M. Ruegg, E. Meier, and D. Nuesch, "Constant motion, acceleration, vibration, and rotation of objects in SAR data," *Proc. SPIE*, vol. 5980, pp. 598005-1–598005-12, Oct. 2005. [Online]. Available: <http://dx.doi.org/10.1117/12.626529>
- [7] M. Ruegg, E. Meier, and D. Nuesch, "Vibration and rotation in millimeter-wave SAR," *IEEE Trans. Geosci. Remote Sens.*, vol. 45, no. 2, pp. 293–304, Feb. 2007.
- [8] V. C. Chen, F. Li, S.-S. Ho, and H. Wechsler, "Micro-Doppler effect in radar: Phenomenon, model, and simulation study," *IEEE Trans. Aerosp. Electron. Syst.*, vol. 42, no. 1, pp. 2–21, Jan. 2006.
- [9] X. Bai, M. Xing, F. Zhou, G. Lu, and Z. Bao, "Imaging of micromotion targets with rotating parts based on empirical-mode decomposition," *IEEE Trans. Geosci. Remote Sens.*, vol. 46, no. 11, pp. 3514–3523, Nov. 2008.
- [10] Q. Wang, M. Xing, G. Lu, and Z. Bao, "High-resolution three-dimensional radar imaging for rapidly spinning targets," *IEEE Trans. Geosci. Remote Sens.*, vol. 46, no. 1, pp. 22–30, Jan. 2008.
- [11] X. B. Li Deng, Y. L. Qin, H. Q. Wang, and Y. P. Li, "The influence of target micromotion on SAR and GMTI," *IEEE Trans. Geosci. Remote Sens.*, vol. 49, no. 7, pp. 2738–2751, Jul. 2011.
- [12] Q. Wang *et al.*, "SAR-based vibration estimation using the discrete fractional Fourier transform," *IEEE Trans. Geosci. Remote Sens.*, vol. 50, no. 10, pp. 4145–4156, Oct. 2012.
- [13] Q. Wang *et al.*, "Demonstration of target vibration estimation in synthetic aperture radar imagery," in *Proc. IEEE Int. Geosci. Remote Sens. Symp.*, Jul. 2011, pp. 4083–4086.
- [14] Q. Wang, M. Pepin, B. Santhanam, T. Atwood, and M. M. Hayat, "SAR-based vibration retrieval using the fractional Fourier transform in slow time," *Proc. SPIE*, vol. 7669, pp. 766911-1–766911-10, Apr. 2010. [Online]. Available: <http://dx.doi.org/10.1117/12.849671>
- [15] Q. Wang, M. M. Hayat, B. Santhanam, and T. Atwood, "SAR vibrometry using fractional Fourier transform processing," *Proc. SPIE*, vol. 7308, pp. 73080B-1–73080B-9, Apr. 2009. [Online]. Available: <http://dx.doi.org/10.1117/12.818370>
- [16] Q. Wang, B. Santhanam, M. Pepin, and M. M. Hayat, "Performance analysis on synthetic aperture radar-based vibration estimation in clutter," in *Proc. Rec. 46th Asilomar Conf. Signals, Syst. Comput. (ASILOMAR)*, Nov. 2012, pp. 217–221.
- [17] J. Adebello and B. Santhanam, "Clutter suppression in synthetic aperture radar targets using the DFRFT and subspace methods with rank reduction," in *Proc. 49th Asilomar Conf. Signals, Syst. Comput.*, Nov. 2015, pp. 1669–1673.
- [18] Y. Chen, B. Deng, H. Wang, Y. Qin, and J. Ding, "Vibration target detection and vibration parameters estimation based on the DPCA technique in dual-channel SAR," *Sci. China Inf. Sci.*, vol. 55, no. 10, pp. 2281–2291, Oct. 2012. [Online]. Available: <https://doi.org/10.1007/s11432-012-4657-9>
- [19] Y. Liang, Q. Zhang, Y. Luo, Y.-Q. Bai, and Y.-A. Chen, "Micro-Doppler features analysis and extraction of vibrating target in FMCW SAR based on slow time envelope signatures," *IEEE Geosci. Remote Sens. Lett.*, vol. 12, no. 10, pp. 2041–2045, Oct. 2015.
- [20] B. Liu, K. Yin, Y. Li, F. Shen, and Z. Bao, "An improvement in multichannel SAR-GMTI detection in heterogeneous environments," *IEEE Trans. Geosci. Remote Sens.*, vol. 53, no. 2, pp. 810–827, Feb. 2015.
- [21] W. Zhang, C. Tong, Q. Zhang, and X. Zhang, "Micro-Doppler extraction of vibrating target based on dual-channel ATI technique in SAR," in *Proc. 2nd IITA Int. Conf. Geosci. Remote Sens.*, vol. 1, Aug. 2010, pp. 422–425.
- [22] Y. Zhang, "Along track interferometry synthetic aperture radar (ATI-SAR) techniques for ground moving target detection," Air Force Res. Lab./SNRT, Fort Belvoir, VA, USA, Tech. Rep. AFRL-SN-RS-TR-2005-410, Jan. 2006. [Online]. Available: <http://www.dtic.mil/dtic/tr/fulltext/u2/a444174.pdf>
- [23] S. Chiu and C. Livingstone, "A comparison of displaced phase centre antenna and along-track interferometry techniques for RADARSAT-2 ground moving target indication," *Can. J. Remote Sens.*, vol. 31, no. 1, pp. 37–51, 2005. [Online]. Available: <http://dx.doi.org/10.5589/m04-052>
- [24] J. G. Vargas-Rubio and B. Santhanam, "An improved spectrogram using the multiangle centered discrete fractional Fourier transform," in *Proc. IEEE Int. Conf. Acoust., Speech, Signal Process. (ICASSP)*, vol. 4, Mar. 2005, pp. IV-505–IV-508.
- [25] H. V. Poor, *An Introduction to Signal Detection and Estimation*. New York, NY, USA: Springer-Verlag, 2013, doi: 10.1007/978-1-4757-2341-0.
- [26] R. E. Kalman, "A new approach to linear filtering and prediction problems," *Trans. ASME, D, J. Basic Eng.*, vol. 82, no. 1, pp. 35–45, 1960.
- [27] S. J. Julier and J. K. Uhlmann, "New extension of the Kalman filter to nonlinear systems," vol. 3, no. 26, pp. 182–193, 1997. [Online]. Available: <http://dx.doi.org/10.1117/12.280797>
- [28] E. A. Wan and R. Van Der Merwe, "The unscented Kalman filter for nonlinear estimation," in *Proc. IEEE Adapt. Syst. Signal Process., Commun., Control Symp.*, Oct. 2000, pp. 153–158.
- [29] R. Fitzgerald, "Divergence of the Kalman filter," *IEEE Trans. Autom. Control*, vol. AC-16, no. 6, pp. 736–747, Dec. 1971.
- [30] D. J. Coe and R. G. White, "Moving target detection in SAR imagery: Experimental results," in *Proc. Int. Radar Conf.*, May 1995, pp. 644–649.
- [31] A. W. Doerry, "Performance limits for synthetic aperture radar," Sandia Nat. Lab., Albuquerque, NM, USA, Sandia Rep. SAND2001-0044, 2001. [Online]. Available: <http://prod.sandia.gov/techlib/access-control.cgi/2001/010044.pdf>
- [32] F. M. Dickey, J. M. DeLaurentis, and A. W. Doerry, "A SAR imaging model for large-scale atmospheric inhomogeneities," *Proc. SPIE*, vol. 5410, pp. 1–9, Aug. 2004. [Online]. Available: <http://dx.doi.org/10.1117/12.541560>
- [33] A. W. Doerry, "Earth curvature and atmospheric refraction effects on radar signal propagation," Sandia Nat. Lab., Livermore, CA, USA, Tech. Rep. SAND2012-10690, 2013.
- [34] A. W. Doerry, "Noise and noise figure for radar receivers," Sandia Nat. Lab., Livermore, CA, USA, Tech. Rep. SAND2016-9649, 2016.
- [35] A. W. Doerry, "Motion measurement for synthetic aperture radar," Sandia Nat. Lab., Livermore, CA, USA, Tech. Rep. SAND2015-20818, 2015.



Justin B. Campbell received the B.S. degree in applied mathematics from the University of Arizona, Tucson, AZ, USA, in 2011, and the M.S. degree in electrical engineering from the University of New Mexico, Albuquerque, NM, USA, in 2016.

His research interests include signal processing, synthetic aperture radars, dual-antenna radar systems, and vibrometry.



Francisco Pérez received the B.S. degree in electronic engineering, the Professional Electronic Engineer certification, and the M.S. degree in electrical engineering from the University of Concepción, Región del Bío-bío, Chile, in 2011, 2013, and 2015, respectively, all with maximum distinction. He is currently pursuing the Ph.D. degree in engineering with an emphasis on electrical engineering with the University of New Mexico, Albuquerque, NM, USA.

His research interests include signal and image processing, imaging systems, infrared detectors, synthetic aperture radars, vibrometry, and their application to pattern recognition problems.



Qi Wang (S'08) received the B.Sc. degree in electrical engineering from Shanghai Jiaotong University, Shanghai, China, in 2007, and the Ph.D. degree in electrical engineering from the University of New Mexico, Albuquerque, NM, USA, in 2012.

His research interests include imaging algorithms for high-resolution synthetic aperture radar (SAR), detection and estimation of nonstatic targets for SAR, and nonstationary signal processing.



Balasubramaniam Santhanam (S'92–M'98–SM'05) received the B.S. degree in electrical engineering from Saint Louis University, Saint Louis, MO, USA, in 1992, and the M.S. and Ph.D. degrees in electrical engineering from the Georgia Institute of Technology, Atlanta, GA, USA, in 1994 and 1998, respectively.

He was a Lecturer and a Post-Doctoral Researcher at the Department of Electrical and Computer Engineering, University of California at Davis, Davis, CA, USA, for one year. He joined the

Department of Electrical and Computer Engineering, University of New Mexico, Albuquerque, NM, USA, in 1999, where he is currently an Associate Professor of electrical and computer engineering and the Gardner-Zemke Professor. His current research interests include discrete fractional Fourier analysis and applications, multicomponent amplitude modulation/frequency modulation models and demodulation, wideband FM demodulation and applications, signal representations for modulated signals, hybrid independent component analysis-support vector machine systems, and their application to pattern recognition problems.

Dr. Santhanam is a member of the IEEE Signal Processing and Communication Society and served as the Chair of the Albuquerque Chapter of the IEEE Signal Processing and Communication Society from 2009 to 2014. He has served as the Technical Area Chair for adaptive systems for the Asilomar Conference on Signals, Systems, and Computers in 2004, and he currently serves on the Conference Steering Committee.



Ralf Dunkel received the B.S., M.S., and Ph.D. degrees from the Martin Luther University of Halle-Wittenberg, Halle, Germany.

He is currently the Director with General Atomics Aeronautical, San Diego, CA, USA, leading the Mission Systems Flight Test Group. His research interests include system qualification, system integration, flight engineering, and flight operations including airborne sensor testing and data analysis.



Armin W. Doerry is currently pursuing the Ph.D. degree in electrical engineering with the University of New Mexico, Albuquerque, NM, USA.

He is a Distinguished Member of Technical Staff with the Surveillance and Reconnaissance Department, Sandia National Laboratories, Albuquerque, NM, USA. He has been involved in numerous aspects of SAR and other radar systems analysis, design, and fabrication since 1987.



Thomas Atwood received the Ph.D. degree from the University of New Mexico, Albuquerque, NM, USA.

He has over 30 years of experience in Engineering Research and Development. Prior to joining the Sandia National Laboratories (SNL), Albuquerque, NM, USA, in 1987, he was involved in several DOD programs, designing/fielding hardware for a variety of aircraft programs. After joining SNL, he contributed to a variety of DOE and DOD projects in areas as diverse as inertial confinement fusion, nuclear weapons transportation, space-borne detection of nuclear explosions, and synthetic aperture radar for proliferation detection. His research interests include the collection, detection, and classification of electromagnetic signatures generated by processes through all phases of the nuclear fuel cycle. He also serves as the Senior Technical Advisor to the Proliferation Detection Program at SNL. He is currently a Research Assistant Professor with the University of New Mexico.



Majeed M. Hayat (F'14) received the B.S. degree (*summa cum laude*) in electrical engineering from the University of the Pacific, Stockton, CA, USA, in 1985, and the M.S. and Ph.D. degrees in electrical and computer engineering from the University of Wisconsin–Madison, Madison, WI, USA, in 1988 and 1992, respectively.

He is currently a Professor of electrical and computer engineering, a member of the Center for High Technology Materials, and the Co-Chair of the Optical Science and Engineering Program with the University of New Mexico, Albuquerque, NM, USA. He has authored or co-authored over 100 peer-reviewed journal articles (nearly 4300 citations) and holds 12 issued patents, five of which have been licensed. He has an H-Index 33. His research interests include resilience and reliability of interdependent cyberphysical systems, dynamical modeling of cascading phenomena with applications to power systems, avalanche photodiodes, statistical communication theory, signal and image processing, algorithms for spectral and radar sensing and imaging, optical communication, and networked computing.

Dr. Hayat was a recipient of the National Science Foundation Early Faculty Career Award in 1998 and the Chief Scientist Award for Excellence in 2006 by the National Consortium for MASINT Research and the Defense Intelligence Agency. He was an Associate Editor of *Optics Express* (Photodetectors and Image Processing) from 2004 to 2010, and an Associate Editor and a member of the Conference Editorial Board for the IEEE Control Systems Society from 2003 to 2008. From 2010 to 2013, he was the Chair of the Topical Committee on Photodetectors, Sensors, Systems, and Imaging of the IEEE Photonics Society. He is currently an Associate Editor of the IEEE TRANSACTIONS ON PARALLEL AND DISTRIBUTED SYSTEMS. He is a fellow of OSA and SPIE.